Frog Skeletal Muscle Thick Filaments Are Three-Stranded

ROBERT W. KENSLER* and MURRAY STEWART‡
*Department of Anatomy, The Medical College of Pennsylvania, Philadelphia, Pennsylvania 19129; ‡Medical Research Council, Laboratory of Molecular Biology, Cambridge CB2 2QH, United Kingdom

ABSTRACT A procedure has been developed for isolating and negatively staining vertebrate skeletal muscle thick filaments that preserves the arrangement of the myosin crossbridges. Electron micrographs of these filaments showed a clear periodicity associated with crossbridges with an axial repeat of 42.9 nm. Optical diffraction patterns of these images showed clear layer lines and were qualitatively similar to published x-ray diffraction patterns, except that the 1/14.3-nm meridional reflection was somewhat weaker. Computer image analysis of negatively stained images of these filaments has enabled the number of strands to be established unequivocally. Both reconstructed images from layer line data and analysis of the phases of the inner maxima of the first layer line are consistent only with a three-stranded structure and cannot be reconciled with either two- or four-stranded models.

Vertebrate skeletal muscle thick filaments are bipolar assemblies of myosin molecules together with small quantities of accessory proteins (2, 8). The rodlike myosin tails constitute the filament backbone, while the globular myosin heads lie on the surface (8). During contraction, the heads form crossbridges with actin in the thin filaments, producing a relative sliding of the two interdigitating filament arrays and so generate tension (7, 10).

An understanding at the molecular level of how tension is generated requires a knowledge of the arrangement and number of myosin heads along the filament. X-ray diffraction studies (6, 9) have established that the myosin heads in vertebrate skeletal muscle thick filaments are arranged approximately helically with an axial repeat of 42.9 nm and with the myosin heads spaced axially by ~14.3 nm. The number of strands in this structure (or the number of myosin heads occurring axially every 14.3 nm) has not been definitively established. Either two-, three-, or four-stranded structures appear to be consistent with the x-ray data, although three-stranded structures are thought to be the most likely (6, 21). Biochemical studies suggest, similarly, that there are either three or four myosin heads per 14.3 nm (17, 19, 24). Quantitative mass measurements by electron microscopy favor three myosin heads per 14.3 nm, but cannot completely exclude two or four myosin heads (15, 20).

It should ideally be possible to determine the number of strands directly by electron microscopy. However, previous studies have encountered difficulties in preserving the ordered structure of the crossbridges during filament isolation and staining (2, 4, 21). We have recently devised conditions that enabled the isolation of thick filaments from several invertebrates (*Limulus*, tarantula, scorpion) with the crossbridge arrangement largely intact (11–13, 16). We have now applied these methods to frog muscle and report here the isolation of these thick filaments with the ordering of their heads substantially preserved. Analysis of electron micrographs of these filaments by both optical and computer methods has enabled us to establish unequivocally that frog skeletal muscle thick filaments are three-stranded.

MATERIALS AND METHODS

Thick filaments were isolated from whole thigh muscles of the frog (*Rana pipiens*) by a modification of the Hardwicke and Hanson technique (5) similar to that previously used to isolate *Limulus* filaments (11). 3–5-mm diameter bundles were quickly snipped from pithed animals and immediately immersed in a relaxing solution containing 0.1 M NaCl, 2 mM EGTA, 1 mM dithiothreitol, 5 mM $MgCl_2$, 2.5 mM ATP, and 7 mM phosphate buffer (pH 7.2) at 4°C. This temperature was maintained during subsequent steps. After 2–5 h the bundles, were changed into fresh solution and left overnight. A bundle was then finely minced with a razor blade and homogenized in relaxing solution in which NaCl was replaced with KCl. Homogenization was carried out on ice with two 15-s bursts (separated by 30 s) at setting 3 of a Sorvall Omnimixer using a 5-ml minicup. The homogenate was diluted with relaxing solution to 15 ml and centrifuged at 3,000 *g* for 10 min. Separated thick filaments remained in the supernatant and were directly adsorbed onto grids coated with a thin (~5–7 nm) carbon film supported on a perforated formvar film and negatively stained with 1% uranyl acetate as described previously (11). Grids were not glow-discharged. Platinum and platinum-carbon shadowing of filaments at an angle of ~30° was performed as described previously (12). Preparations were examined in a Philips EM 300 electron microscope at 80 kV with an anticontamination device in use. Magnification was calibrated by using catalase crystals (26) or tropomyosin tactoids (1). Micrographs were examined by eye to select areas in which the filaments appeared to be straight and uncontaminated by debris and these filaments were examined by optical diffraction as described previously (11).

Computer image processing was performed using essentially the same Fourier-based methods used to examine *Limulus* thick filaments (23). These methods and their general theoretical basis have been reviewed elsewhere (3). Briefly, filaments that showed a clear first layer line at 43 nm^{-1} and a meridional reflection at 14.3 nm^{-1} were digitized at intervals corresponding to ~1 nm on the original object, and the required area was windowed off. After reducing average edge density to

zero and inserting a Gaussian edge apodization (corresponding to a variance of 3 nm), the matrix was embedded into a 256 × 512 array of zeros and its Fourier transform was computed. When necessary, a new image density raster was interpolated from the original data to ensure that the layer lines in the Fourier transform were parallel to the sampling raster and that the layer lines lay on raster lines rather than between them. Reconstructed images were produced by Fourier inversion. Phase origins were initially taken at the center of the particle and then refined so that the mean amplitude-weighted phase difference between

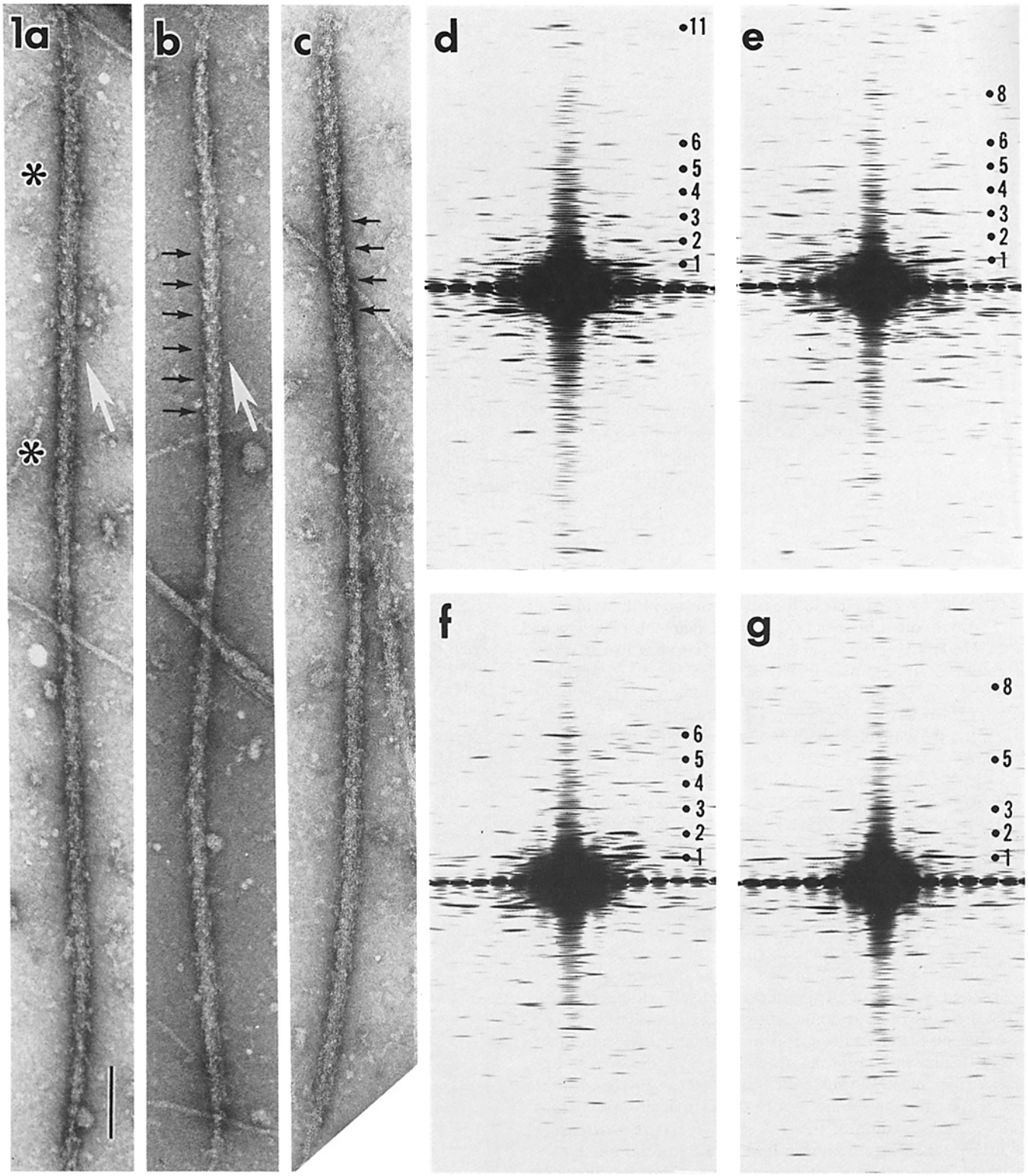

FIGURE 1 *a–c* Electron micrographs of frog thick filaments negatively stained with 1% uranyl acetate. An axial periodicity can be seen by sighting along the filament axes (*a–c*), while helical stripes can be seen by sighting along the white arrowheads in *a* and *b*. Arrows in *b* and *c* indicate crossbridges projecting axially from the filament backbone every ~43 nm. The region between asterisks in *a* is typical of the regions examined by optical diffraction. Bar, 0.1 μm. × 125,500. *d–g* Optical diffraction patterns obtained from filaments such as those shown in *a–c*. The patterns show a clear series of layer lines indexing on a 43-nm repeat. There is a clear meridional reflection on the third layer line and there are also meridional reflections on layer lines 2, 5, 8, and 11 that would not be expected if the filament were completely helical.

corresponding points on the equator was zero and between corresponding points on the first layer line either zero or 180° (whichever was closer). No assumptions were made about the number of strands.

RESULTS

Appearance of Frog Thick Filaments in Electron Micrographs

The filament isolation procedure described above yielded populations of frog thick filaments that were uniform in length (1.53 ± 0.05 μm SD, n = 24), with ordered arrays of crossbridges. Even on low magnification electron micrographs, negatively stained filaments showed a clear periodicity along their length, except for a central bare zone that was 149 ± 13 nm (SD, n = 19) long. At higher magnifications (Fig. 1, *a–c*) the periodic arrangement of crossbridges can be seen more clearly by tilting the micrographs and looking along the length of a filament, while the helical striping of the filaments can be seen by viewing from an angle (along the white arrows in Fig. 1, *a* and *b*). Crossbridges normally seemed to be closely apposed to the filament backbone and only slightly tilted from the filament axis, although they were sometimes seen projecting away from the filament (Fig. 1, *b* and *c*). The maximum filament diameter measured in the crossbridge region averaged 29.1 ± 2.1 nm (SD, n = 475), whereas the diameter at the bare zone averaged 15.8 ± 1 nm (SD, n = 55). If one takes the diameter of the bare zone as indicative of the diameter of the shaft of the thick filament, then this would imply that the crossbridges extended ~7 nm from the surface of the shaft and were probably centered at a radius of ~11.2 nm. This is in good agreement with previous estimates based on x-ray diffraction data (6). "End filaments" very similar to those seen in rabbit thick filaments (25) could often be seen at the tips of filaments (Fig. 1, *a* and *b*). Dr. R. Craig (personal communication) has also seen these structures in frog thick filaments. The end filaments observed here had a distinct cross striation of 4.3 ± 0.12 nm (SD, n = 22) similar to that observed in rabbit (25).

Frog thick filaments showed a clear, right-handed, approximately helical arrangement of cross bridges when shadowed with either platinum or platinum-carbon after being first rinsed briefly with uranyl acetate (Fig. 2). Filaments appeared ropelike with strands running diagonally across them at intervals of ~43 nm. This ropelike structure extended uniformly across both arms of the filaments but was absent along the bare zone, which is consistent with the interpretation that these strands corresponded to the paths followed by the crossbridges.

Optical Diffraction Analysis

Many electron micrographs of negatively stained frog thick filaments gave clear optical diffraction patterns (Fig. 1, *d–g*) similar to those obtained by x-ray diffraction (6, 9) from frog muscle. In well preserved specimens, a series of layer lines, indexing on a 42.9-nm repeat, typically extended to at least the 6th layer line and frequently to the 11th layer line (Table I). The inner maxima of the first layer line were always much stronger than the other layer lines in the pattern, which paralleled the distribution of intensity seen in x-ray diffraction patterns (6). The intensity of the second maximum on the first layer line was variable and was often different in intensity on opposite sides of the layer line. A meridional reflection on the third layer line was consistently present although somewhat weaker than the corresponding reflection in x-ray diffraction patterns (6, 9). Subsidiary maxima were frequently observed along the third layer line. Additional meridional reflections, not expected if the structure was entirely helical, were often present on the 2nd, 5th, 8th, and 11th layer lines and, less frequently, on the 4th, 7th, and 10th layer lines (Fig. 1, *d–g*). A similar pattern of so-called "forbidden" meridional reflections is also seen in x-ray diffraction patterns from frog muscle (9, 27) and in optical transforms of cryosectioned human muscle (22) and indicates some departure from strict helical symmetry.

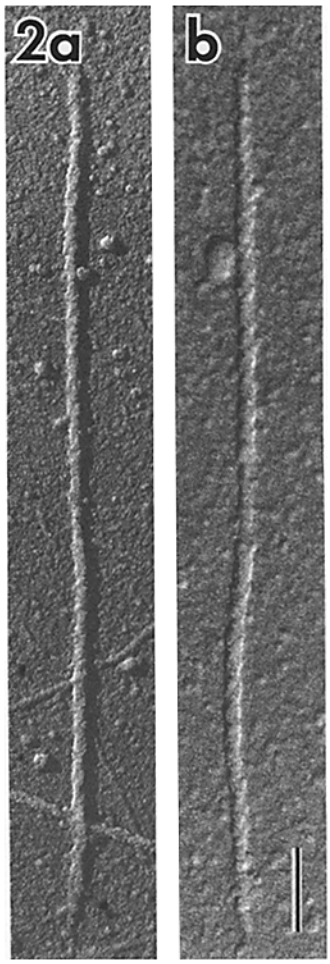

FIGURE 2 Electron micrographs of filaments unidirectionally shadowed with platinum (*a*) and platinum-carbon (*b*) after washing with uranyl acetate. The approximately helical strands are right-handed and can be most clearly seen by sighting along the filament axes. Bar, 0.15 μm. × 75,200.

TABLE I

Layer Line Spacings in Optical Diffraction Patterns *

Layer line	Spacing	Number of observations	Deviation of mean value from 42.9 nm/L
(L)	*mean ± SD*		%
1	42.8 ± 0.6	25	0.2
2	21.6 ± 0.2	25	0.3
3	14.3	25	—
4	10.7 ± 0.1	25	0.2
5	8.6 ± 0.1	23	0.2
6	7.2 ± 0.1	20	0.2
7	6.2 ± 0.1	16	1.1
8	5.4 ± 0.1	18	0.7
9	4.8 ± 0.1	10	0.6
10	4.3 ± 0.03	6	0.2
11	3.9 ± 0.03	16	0

* Normalized by taking the spacing of the third layer line meridional reflection as 1/14.3 nm^{-1}

The inner maxima on the first, second, fourth, and fifth layer lines were all found at a radial spacing of $\frac{1}{16}$–$\frac{1}{17}$ nm^{-1} (Table II), which was reasonably close to the radial spacing of ~$\frac{1}{20}$ nm^{-1} estimated from x-ray data (6, 9). One can estimate the number of strands (N) from the position of these inner maxima, since they will all derive from Bessel functions of order N. Helical diffraction theory (14) indicates that the radial position of the maximum (R) depends on both N and the radial position of the center of mass of the crossbridge (r). If one takes r as 11.2 nm (i.e., midway between the radius of the filament shaft and the maximum filament radius seen in the crossbridge region) and R as $\frac{1}{17}$ nm^{-1}, then $2\pi rR = 4.0$. This is close to the value expected (4.2) for a J_3 Bessel function, which would correspond to a three-stranded structure, whereas values of 3.1 and 5.3 would be expected for two- and four-stranded structures. However, this calculation is only approximate and it is not possible to rule out two- or four- stranded structures on this basis alone.

Computer Image Processing

Additional evidence for a three-stranded structure was obtained by computer image processing. Individual crossbridges on the filament surface were not sufficiently clear in the original micrographs to enable an unequivocal assignment to be made. Although one could make out some crossbridges quite clearly, others were obscured by image noise or disorder or were made difficult to see by the density associated with the filament backbone. To circumvent these problems, images were reconstructed using all the data on the first six layer lines. The contribution from the equator was also omitted, and this had the effect mainly of removing the density associated with the filament backbone, making it easier to identify individual crossbridges. There was no masking of data across layer lines, so this operation strictly involved only the assumption that the structure was repeated axially every 43 nm. Neither a $3N$-fold screw axis nor even helical symmetry was assumed and absolutely no assumptions about the number of strands were implicit in this reconstruction.

Fig. 3 shows reconstructed images from six filaments. In each filament, three approximately helical tracks can be made out, although the individual subunits along each track were not always completely resolved. The filament in Fig. 3 *a* showed mainly one side of the filament, presumably as a result of uneven negative staining, and this enabled the helical paths to be made out most clearly as there was then little interference from the other side of the filament. The remainder of the filaments shown in Fig. 3 had approximately equal contributions from both sides of the filament. Although there was some superposition of patterns from the top and bottom of the structure, it was still quite easy to trace three helical paths in these images. One cannot reasonably draw either two or four

TABLE II

Radial Spacing of Inner Layer Line Maxima in Optical Diffraction Patterns

Layer line	Radial position of maximum	Number of observations
(L)	*nm^{-1} ± SD*	
1	17.7 ± 2.0	50
2	17.8 ± 2.3	48
4	17.4 ± 2.2	35
5	16.5 ± 1.8	24

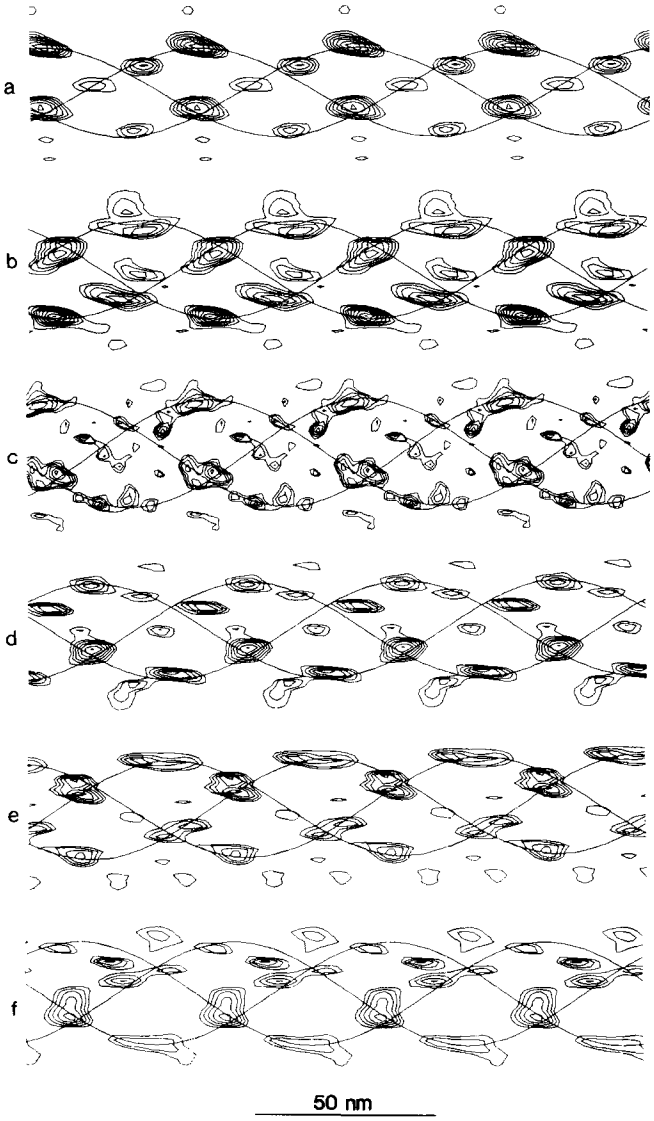

FIGURE 3 Reconstructed thick filament images using the first six layer lines and omitting the equator. In each image, three approximately helical tracks can be drawn. Only positive contours, corresponding to areas of high protein density, are shown. Bar, 50 nm.

helical tracks through the data in Fig. 3 and, furthermore, the images strikingly lack the mirror symmetry that would be required if the number of strands were even. A similar lack of mirror symmetry was also apparent in the micrographs (Fig. 1).

Confirmation of the three-stranded structure was obtained from an examination of the computed Fourier transforms of these particles. Helical diffraction theory (14) and also a more general formulation in terms of cylindrical diffraction (which takes account of departures from helical symmetry) requires that the inner maxima on the first layer line be sums of Bessel functions of order N, where N is the number of helical strands. Provided the phase origin is located on the helical axis, the phase difference between the reflections on the opposite sides of the layer line will ideally be $N \times 180°$. Thus, the phase difference between opposing maxima would be zero if the number of helical strands were even, and 180° if the number were odd. Fig. 4 shows the amplitude and phase data on the first layer line from a single filament and clearly the inner maxima are close to 180° out of phase. For the six particles

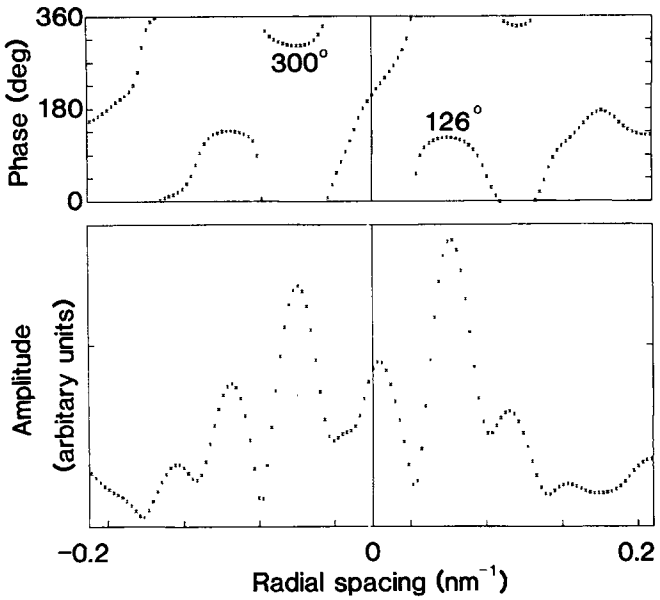

FIGURE 4 Amplitude and phase data across the first layer line from the computed Fourier transform of a single thick filament. The inner maxima are clearly close to 180° out of phase.

examined, the phase differences of the opposing inner maxima on the first layer line were 152, 161, 166, 169, 174, and 178°. This was only consistent with a three-stranded helix and definitively excluded two- and four-stranded structures.

DISCUSSION

The results presented here demonstrate that we have isolated negatively stained thick filaments from frog skeletal muscle in which the approximately helical arrangement of the crossbridges has been largely preserved. The optical diffraction patterns from electron micrographs of these filaments generally resembled those obtained by low-angle x-ray diffraction of living, whole relaxed muscle (6, 9). Both optical and x-ray diffraction patterns show a similar series of layer lines indexing on a 42.9-nm repeat. In x-ray diffraction patterns, these layer lines have been interpreted as arising from the approximately helical arrangement of the myosin crossbridges (9). In addition, the optical diffraction patterns show the "forbidden" meridional reflections seen in x-ray data. The intensity of the 14.3-nm meridional reflection on the third layer line was consistently weaker in our patterns than has been observed in x-ray patterns. It is extremely unlikely that this indicates that the number of strands had changed during filament preparation, but instead it may reflect a change in crossbridge orientation so that the projected axial density modulation per 14.3 nm is reduced or may derive from lattice sampling in x-ray patterns (Dr. H. E. Huxley, personal communication). Thus, the overall similarity of the x-ray and optical diffraction patterns indicated that the native order of the myosin crossbridges had been largely preserved during filament isolation and staining and so the appearance of the filaments in the micrographs reflected their structure in situ reasonably well.

The degree of preservation of the ordered structure of the crossbridges in these frog thick filaments was sufficient to enable us to establish unequivocally that frog thick filaments are three-stranded. Although initially two-stranded models were proposed for vertebrate skeletal muscle thick filaments (9, 18), recent interpretations of x-ray data have suggested that more likely there are three strands in the structure (6, 21). This would be consistent with biochemical studies that indicated either three or four myosin molecules per 14.3 nm (17, 19, 24) and with mass measurements made by scanning transmission electron microscopy (15, 20), which were most consistent with three myosins per 14.3 nm.

It has recently been proposed that the forbidden meridional reflections may derive from a fluctuation in the axial position of the crossbridges (22, 27). The general appearance of the translationally averaged images (Fig. 3) is certainly consistent with this idea: one obtains the distinct impression that two successive 14.3-nm levels are closely grouped together and separated more widely from the remaining level in the 42.9-nm repeat. Furthermore, the crossbridges in this remaining level appear to be more dense, possibly reflecting the presence of C-protein. However, confirmation of these points will have to await more extensive analysis.

This study has only determined the number of approximately helical strands and thus the number of crossbridges per 14.3 nm in frog thick filaments. The interaction between Bessel functions of orders 3 and 6 on layer lines 1 and 2, combined with the small but undoubted departure from helical symmetry implied by the forbidden meridional reflections, makes it difficult to produce one-sided images or three-dimensional reconstructions. More detailed information of shape will have to await decomposition of the Fourier transform, which will require analysis of tilt series. Finally, we stress that, while our data have established the number of strands in these filaments, it does not give any information regarding the packing of the myosin tails into the filament shaft. To conclude from our data that the tails were arranged in an approximately helical manner similar to that of the heads would not be justified, and we caution readers that our results should not be used to attempt to decide between competing models of backbone structure. There is some substructure present in the shaft region on some of our micrographs, and we are analyzing these images to see whether any reliable data regarding packing can be obtained.

We thank our colleagues in Philadelphia and Cambridge, particularly Rhea Levine, Hugh Huxley, Aaron Klug, and Tony Crowther for their many helpful comments and criticisms.

This work was supported in part by U. S. Public Health Service Grant AM30442 to Dr. Kensler.

Received for publication 1 February 1983.

REFERENCES

1. Caspar, D. L. D., C. Cohen, and W. Longley. 1969. Tropomyosin: crystal structure polymorphism and molecular interactions. *J. Mol. Biol.* 41:87–97.
2. Craig, R. 1977. Structure of A-segments from frog and rabbit skeletal muscle. *J. Mol. Biol.* 109:69–81.
3. Crowther, R. A., and Klug, A. 1975. Structural analysis of macromolecular assemblies by image reconstruction from electron micrographs. *Annu. Rev. Biochem.* 44:161–182.
4. Hanson, J., E. J. O'Brien, and P. M. Bennett. 1971. Structure of the myosin-containing filament assembly (A-segment) separated from frog skeletal muscle. *J. Mol. Biol.* 58:865–871.
5. Hardwicke, P. M. D., and J. Hanson. 1971. Separation of thick and thin myofilaments. *J. Mol. Biol.* 59:509–516.
6. Haselgrove, J. C. 1980. A model of myosin cross-bridge structure consistent with the low angle X-ray diffraction pattern of vertebrate muscle. *J. Muscle Res. Cell Motil.* 1:177–191.
7. Huxley, A. F., and R. Niedergerke. 1954. Structural changes in muscle during contraction. Interference microscopy of living muscle fibers. *Nature (Lond.).* 173:971–972.
8. Huxley, H. E. 1963. Electron microscope studies of the structure of natural and synthetic protein filaments from muscle. *J. Mol. Biol.* 7:281–308.
9. Huxley, H. E., and W. Brown. 1967. The low-angle X-ray diagram of vertebrate striated muscle and its behavior during contraction and rigor. *J. Mol. Biol.* 30:383–434.
10. Huxley, H. E., and J. Hanson. 1954. Changes in the cross-striations of muscle during contraction and stretch and their structural interpretation. *Nature (Lond.).* 173:973–976.
11. Kensler, R. W., and R. J. C. Levine. 1982. An electron microscopic and optical diffraction analysis of the structure of *Limulus* telson muscle thick filaments. *J. Cell Biol.* 92:443–451.
12. Kensler, R. W., and R. J. C. Levine. 1982b. Determination of the handedness of the crossbridge helix of *Limulus* thick filaments. *J. Muscle Res. Cell Motil.* 3:349–361.

13. Kensler, R. W., R. J. C. Levine, M. Reedy, and W. Hoffmann. 1982. Arthropod thick filament structure. *Biophys. J.* 37(2, Pt. 2):34*a*. (Abstr.)
14. Klug, A., F. H. C. Crick, and H. W. Wyckoff. 1958. Diffraction by helical structures. *Acta Crystallogr.* 11:199–213.
15. Lamvik, M. K. 1978. Muscle thick filament mass measured by electron scattering. *J. Mol. Biol.* 122:55–68.
16. Levine, R. J. C., R. W. Kensler, M. Stewart, and J. C. Haselgrove. 1982. Molecular organization of *Limulus* thick filaments. *In* Basic Biology of Muscles: A Comparative Approach. B. M. Twarog, R. J. C. Levine, and M. M. Dewey, editors. Raven Press, New York. 37–52.
17. Morimoto, K., and W. F. Harrington. 1974. Substructure of the thick filament of vertebrate striated muscle. *J. Mol. Biol.* 83:83–97.
18. Pepe, F. A. 1971. Structure of the myosin filament in striated muscle. *Prog. Biophys. Mol. Biol.* 22:77–96.
19. Pepe, F. A., and B. Drucker. 1979. The myosin filament. VI. Myosin content. *J. Mol. Biol.* 130:379–393.
20. Reedy, M. K., K. R. Leonard, R. Freeman, and T. Arad. 1981. Thick myofilament mass determination by electron scattering measurements with the scanning transmission electron microscope. *J. Muscle Res. Cell Motil.* 2:45–64.
21. Squire, J. M. 1981. The Structural Basis of Muscle Contraction. Plenum Publishing Co., Ltd., London. 225–521.
22. Squire, J. M., J. J. Harford, A. C. Edman, and M. Sjostrom. 1982. Fine structure of the A-band in cryo-sections. III. Crossbridge distribution and the axial structure of the human C-zone. *J. Mol. Biol.* 155:467–494.
23. Stewart, M., R. W. Kensler, and R. J. C. Levine. 1981. Structure of *Limulus* telson muscle thick filaments. *J. Mol. Biol.* 153:781–790.
24. Tregear, R. T., and J. M. Squire. 1973. Myosin content and filament structure in smooth and striated muscle. *J. Mol. Biol.* 77:279–290.
25. Trinick, J. 1981. End-filaments, a new structural element of vertebrate skeletal muscle thick filaments. *J. Mol. Biol.* 151:309–314.
26. Wrigley, N. G. 1968. The lattice spacing of crystalline catalase as an internal standard of length in electron microscopy. *J. Ultrastruct. Res.* 24:454–464.
27. Yagi, N., E. J. O'Brien, and I. Matsubara. 1981. Changes of thick filament structure during contraction of frog striated muscle. *Biophys. J.* 33:121–138.